Supercapacitors of Nanocrystalline Metal–Organic Frameworks

Kyung Min Choi,[†,‡] Hyung Mo Jeong,[‡] Jung Hyo Park,[‡] Yue-Biao Zhang,[†] Jeung Ku Kang,[‡,§,*] and Omar M. Yaghi[†,§,∥,*]

[†]Department of Chemistry, University of California-Berkeley, Materials Sciences Division at Lawrence Berkeley National Laboratory, and Kavli Energy NanoSciences Institute at Berkeley, Berkeley, California 94720, United States, [‡]Department of Materials Science and Engineering and [§]Graduate School of Energy, Environment, Water and Sustainability, Korea Advanced Institute of Science and Technology, 373-1, Guseong Dong, Yuseong Gu, Daejeon 305-701, Republic of Korea, and [∥]Department of Chemistry, King Fahd University of Petroleum and Minerals, Dhahran 34464, Saudi Arabia

ABSTRACT The high porosity of metal–organic frameworks (MOFs) has been used to achieve exceptional gas adsorptive properties but as yet remains largely unexplored for electrochemical energy storage devices. This study shows that MOFs made as nanocrystals (nMOFs) can be doped with graphene and successfully incorporated into devices to function as supercapacitors. A series of 23 different nMOFs with multiple organic functionalities and metal ions, differing pore sizes and shapes, discrete and infinite metal oxide backbones, large and small nanocrystals, and a variety of structure types have been prepared and examined. Several members of this series give high capacitance; in particular, a zirconium MOF exhibits exceptionally high capacitance. It has the stack and areal capacitance of 0.64 and 5.09 mF cm^{-2}, about 6 times that of the supercapacitors made from the benchmark commercial activated carbon materials and a performance that is preserved over at least 10000 charge/discharge cycles.

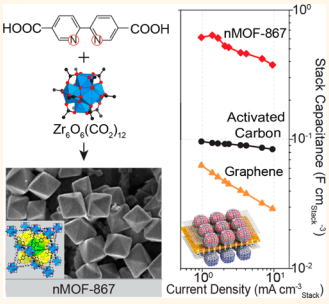

KEYWORDS: metal–organic frameworks · nanocrystals of MOFs · electrochemical capacitors

Electrochemical capacitors, also known as supercapacitors, represent an important class of energy storage devices because of their high power density.[1,2] Porous carbon materials such as activated carbon are commercial supercapacitors that operate by storing charge on electrochemical double layers (EDLs).[3−5] This is in contrast to the storage of charge by redox reactions as exemplified by metal oxide pseudocapacitors.[6−8] Each of these classes of supercapacitors has strengths and weaknesses: carbon-based materials operate at a very high charge/discharge rate with a long life cycle but have low capacitance, while metal oxide materials have high capacitance but their redox reactions lead to low life cycle.[1]

In this study, we show how metal–organic frameworks (MOFs)[9] can be integrated into supercapacitor devices and the flexibility with which their metal oxide and organic constituents can be varied and used to uncover their high capacitance and long life cycle behavior; both are desirable features and sought after in supercapacitor research. We examined a series of 23 different MOF compounds, made in their nanocrystalline form, and chosen for their variability in structure type, organic functionality, geometry and size of metal-containing unit, size of pore, and size of the nanocrystals. Thin film devices prepared from these nanocrystalline MOFs (nMOFs) and doped with graphene give a wide range of stack capacitance (0.025 to 0.64 F cm^{-3}). A member of the series, $Zr_6O_4(OH)_4(BPYDC)_6$ (BPYDC = 2,2′-bipyridine-5,5′-dicarboxylate, termed nMOF-867), has sp^2 nitrogen atoms in the organic link and exhibits the highest stack and areal performance (0.64 and 5.09 mF cm^{-2})—26 times that of the lowest performing member of the series $[Zn_4O(BDC)_{1.67}(C_4H_4–BDC)_{1.33}$ (BDC = 1,4-benzenedicarboxylate), nMTV-MOF-5-AF (MTV = multivariate)] and six times that of commercial activated carbon. We further show that the exceptional performance of nMOF-867 is preserved over at least 10000 cycles. These findings constitute an important step in deploying the rich MOF chemistry for the development of supercapacitors.

In addition to porous carbon and metal oxide materials, porous polymers have been investigated as supercapacitor and found to undergo chemical degradation, thus adversely affecting their life cycle and performance.[10] There is only one study involving the use

* Address correspondence to jeung@kaist.ac.kr, yaghi@berkeley.edu.

Received for review May 18, 2014 and accepted July 7, 2014.

Published online July 07, 2014
10.1021/nn5027092

of a MOF material [Co8-MOF-5, $Zn_{3.68}Co_{0.32}O(BDC)_3$-$(DEF)_{0.75}$], which was found to have much lower capacitance than commercial activated carbon.[11] In the present report, we show that the ability to design nMOFs has led us to overcome these challenges and ultimately access nMOF based supercapacitors with superior performance.

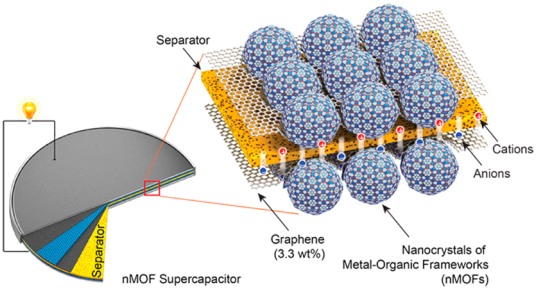

Scheme 1. Construct for nMOF Supercapacitors

RESULTS

Our construct for incorporating nanocrystals of MOFs into supercapacitors is illustrated in Scheme 1. It is based on a coin-type device composed of films made from nMOFs doped with graphene. The films are placed on both sides of a separator membrane and soaked by a solution of an electrolyte. It is expected that by charging the device, the positive and negative ions of the electrolyte move in opposite directions through the separator and into the MOF pores. During discharge, the ions migrate out of the pores and the electrons flow out of the device. MOFs would perform

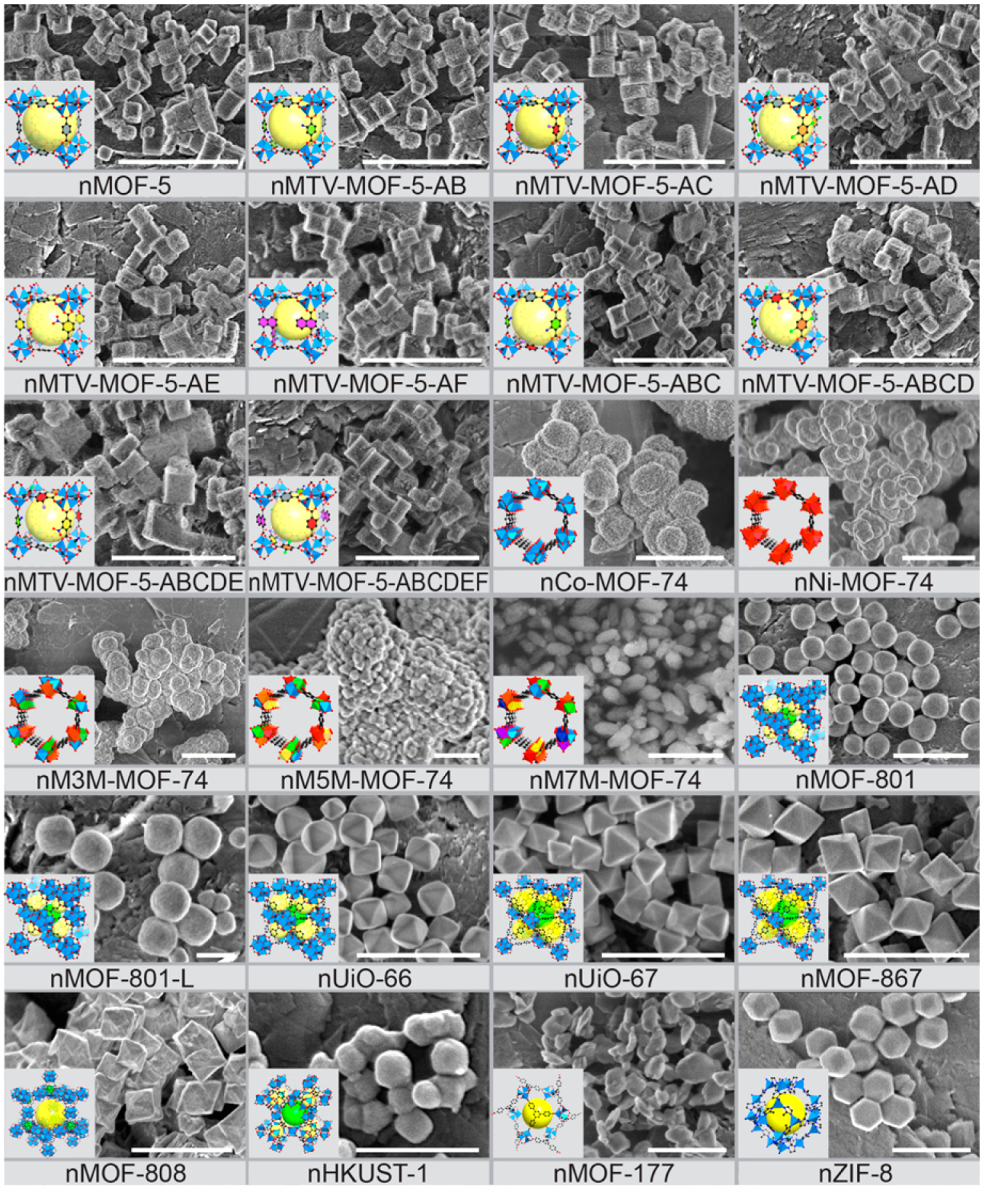

Figure 1. Scanning electron microscopy (SEM) images of the nMOFs (scale bar: 500 nm). Insets are crystal structures for each of the nMOFs. Key: A, BDC, 1,4-benzenedicarboxylate; B, NH_2-BDC; C, Br-BDC; D, $(Cl)_2$-BDC; E, (NO_2)-BDC and F, C_4H_4-BDC; M3M-, $Co_{0.82}Mg_{0.42}Ni_{0.76}$; M5M-, $Co_{0.54}Mg_{0.27}Ni_{0.60}Zn_{0.34}Mn_{0.35}$; M7M-, $Co_{0.23}Mg_{0.13}Ni_{0.20}Zn_{0.16}Mn_{0.16}Fe_{0.11}Cd_{0.03}$.

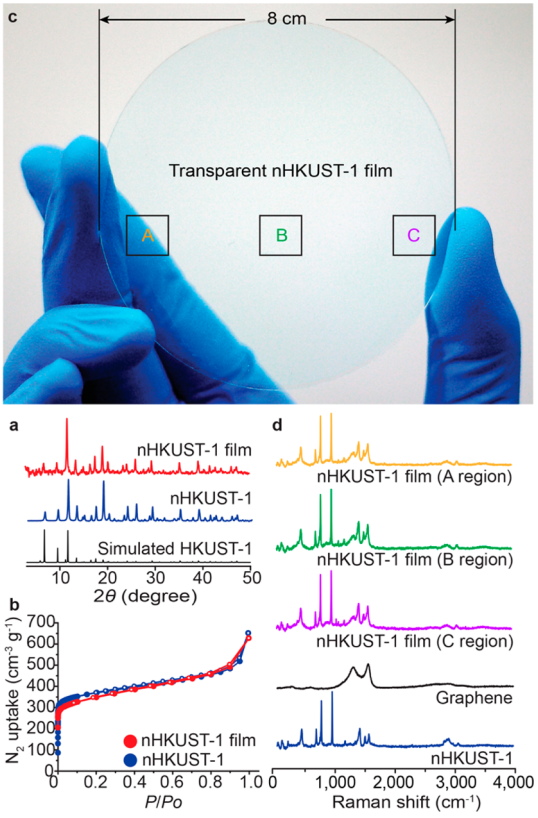

Figure 2. (a) X-ray diffraction patterns of nHKUST-1 and nHKUST-1 film. (b) N_2 adsorption isotherms for the nHKUST-1 and nHKUST-1 film at 77 K with adsorption and desorption points represented by solid and open circles, respectively. P/P_0, relative pressure. (c) A large, transparent nHKUST-1 film on a quartz substrate 8 cm in diameter. (d) Raman spectroscopy from the three points marked as A, B, and C in Figure 1c as well as pristine nHKUST-1 and graphene.

well in this context because of their high porosity and openness of their structure, which should give high capacity for storage of ions and robust cycling of ions within the cell, respectively.[12]

We chose 23 different MOFs and made them in nanocrystalline form (Figure 1): (**1**) $Zn_4O(BDC)_3$ (BDC = 1,4-benzenedicarboxylate), MOF-5,[13] (**2**) $Zn_4O(BDC)_2(NH_2\text{-}BDC)$, MTV-MOF-5-AB, (**3**) $Zn_4O(BDC)_{1.71}(Br\text{-}BDC)_{1.29}$, MTV-MOF-5-AC, (**4**) $Zn_4O(BDC)_{2.03}[(Cl)_2\text{-}BDC]_{0.97}$, MTV-MOF-5-AD, (**5**) $Zn_4O(BDC)_{2.38}(NO_2\text{-}BDC)_{0.62}$, MTV-MOF-5-AE, (**6**) $Zn_4O(BDC)_{1.67}(C_4H_4\text{-}BDC)_{1.33}$, MTV-MOF-5-AF, (**7**) $Zn_4O(BDC)_{1.36}(NH_2\text{-}BDC)_{0.76}(Br\text{-}BDC)_{0.88}$, MTV-MOF-5-ABC, (**8**) $Zn_4O(BDC)_{1.20}(NH_2\text{-}BDC)_{0.67}(Br\text{-}BDC)_{0.72}[(Cl)_2\text{-}BDC]_{0.41}$, MTV-MOF-5-ABCD, (**9**) $Zn_4O(BDC)_{1.10}(NH_2\text{-}BDC)_{0.09}(Br\text{-}BDC)_{0.88}[(Cl)_2\text{-}BDC]_{0.49}(NO_2\text{-}BDC)_{0.44}$, MTV-MOF-5-ABCDE, (**10**) $Zn_4O(BDC)_{0.88}(NH_2\text{-}BDC)_{0.01}(Br\text{-}BDC)_{0.67}[(Cl)_2\text{-}BDC]_{0.44}(NO_2\text{-}BDC)_{0.38}(C_4H_4\text{-}BDC)_{0.62}$, MTV-MOF-5-ABCDEF,[14] (**11**) $Co_2(DOT)$ (DOT = 2,5-dihydroxy-1,4-benzenedicarboxylate), Co-MOF-74,[15] (**12**) $Ni_2(DOT)$, Ni-MOF-74,[15] (**13**) $Co_{0.82}Mg_{0.42}Ni_{0.76}(DOT)$, M3M-MOF-74 (M3M = mixed three metals),[16] (**14**) $Co_{0.54}Mg_{0.27}Ni_{0.60}Zn_{0.34}Mn_{0.35}(DOT)$, M5M-MOF-74,[16] (**15**) $Co_{0.23}Mg_{0.13}Ni_{0.20}Zn_{0.16}Mn_{0.16}Fe_{0.11}Cd_{0.03}(DOT)$, M7M-MOF-74,[16] (**16**) $Zr_6O_4(OH)_4(fumarate)_6$, MOF-801,[17] (**17**) $Zr_6O_4(OH)_4(BDC)_6$, UiO-66,[18] (**18**) $Zr_6O_4(OH)_4(BPDC)_6$ (BPDC = 4,4′-biphenyldicarboxylate), UiO-67,[18] (**19**) $Zr_6O_4(OH)_4(BPYDC)_6$, MOF-867,[19] (**20**) $Zr_6O_4(OH)_4(BTC)_2(HCOO)_6$ (BTC = 1,3,5-benzenetricarboxylate), MOF-808,[20] (**21**) $Cu_3(BTC)_2$, HKUST-1,[21] (**22**) $Zn_4O(BTB)_2$ (BTB = benzene-1,3,5-tribenzoate), MOF-177,[22] (**23**) $Zn(MeIM)_2$ (MeIM = imidazolate-2-methyl), ZIF-8.[23] MOFs listed as **1**−**10** have the same MOF-5 structure with three-dimensional pores and variously mixed functionalities, **11**−**15** are based on the MOF-74 structure with one-dimensional pores and mixed multimetallic metal oxide units, **16**−**20** are zirconium(IV) MOFs differing in the length and shape of their links and the size of their nanocrystals, and **21**−**23** are MOFs with varying nuclearity of the metal containing units.

nMOFs were made by adding the appropriate metal salt to a *N*,*N*-dimethylformamide (DMF) solution of the acid form of the appropriate organic link followed by heating or microwave for a given period of time (Supporting Information). In cases where the metal salt is not that of the acetate, a modulator such as acetic acid or formic acid was added to control the crystal size. The nanocrystals were isolated by centrifuge, washed with a polar organic solvent, and then dried under vacuum. Samples of nMOFs thus produced were characterized by powder X-ray diffraction (PXRD) techniques to confirm their crystallinity and show that they have the same structure as the corresponding original bulk MOFs. Scanning electron microscopy (SEM) was used to determine the size of the nanocrystals (Figure 1). Nitrogen gas adsorption isotherms were measured to confirm the porosity of the samples.

Here, we outline the preparation, characterization, and fabrication of the film and device for the specific case of nHKUST-1 as this procedure was followed for the 23 nMOFs. Samples of nHKUST-1 were prepared by simultaneously adding a solution of 1,3,5-benzenetricarboxylic acid (126 mg, 0.600 mmol) with triethylamine (0.25 mL, 1.8 mmol) in 2 mL of DMF and a solution of $Cu(OAc)_2 \cdot H_2O$ (215 mg, 1.08 mmol) in 5 mL of DMF to a solvent mixture containing DMF (18 mL), EtOH (25 mL), and H_2O (25 mL). After 1 h of stirring, the product was collected using a centrifuge (9000 rpm, 20 min), washed with DMF (2 × 30 mL) and acetone (3 × 30 mL), and then dried *in vacuo* overnight. The crystallinity of nHKUST-1 was examined by PXRD, which gave sharp diffraction peaks matching those of the simulated pattern obtained from experimental X-ray single-crystal diffraction data (Figure 2a). The SEM of the product showed an average crystal size of 100 nm with a size distribution of 20% (Figure 1). The permanent porosity was confirmed by measuring the nitrogen gas sorption isotherm. It showed a shape similar to that observed for this MOF (Figure 2b) and gave a BET surface area of 1470 $m^2\ g^{-1}$, a value within the range found for bulk HKUST-1 (1264 $m^2\ g^{-1}$ to 1507 $m^2\ g^{-1}$).[24,25]

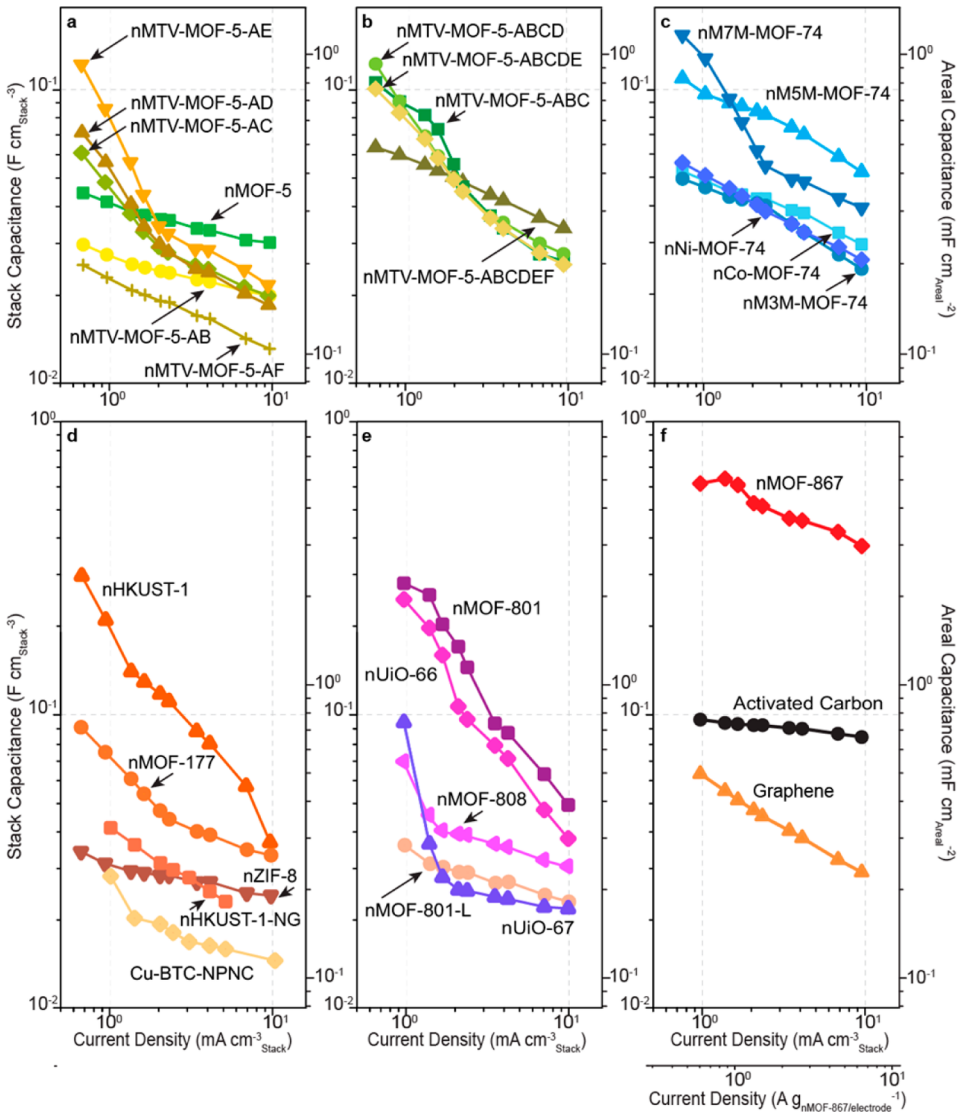

Figure 3. Volumetric stack and areal capacitance of nMOFs and related supercapacitors: (a) nMOFs based on multivariate (MTV) MOF-5 structure with three-dimensional pores and various functionalities and (b) mixed functionalities; (c) nMOF-74s with one-dimensional pores and mixed multimetallic metal oxide units; (d) nMOFs with variable metal oxide nuclearity and comparison of nHKUST-1 supercapacitors with nonporous and noncrystalline and no graphene constituents; (e) zirconium(IV) nMOFs differing in the length and shape of their links and the size of their nanocrystals; (f) highest nMOF supercapacitor (nMOF-867) and comparison to activated carbon and graphene.

The dried nHKUST-1 (70.0 mg) was dispersed with 53 μL of oleic acid in 4.6 mL of hexane under ultrasonication for 3 h. After the nHKUST-1 was separated from 1.0 mL of dispersion using a centrifuge (9000 rpm, 10 min), it was redispersed into 1.0 mL of hexane solution containing 0.5 mg mL^{-1} of graphene (3.3 wt % relative to nHKUST-1) previously dispersed by tip-sonic processor. This colloidal solution of nHKUST-1 and graphene was spread on cleaned titanium substrates and assembled into thin films of nHKUST-1 by using a spin-coating process (7000 rpm, 2 min). Finally, oleic acid was removed by immersing the nHKUST-1 film in acetone, drying with nitrogen flow, and outgassing at room temperature for 12 h (Supporting Information). This fabrication procedure yielded translucent blue nHKUST-1 thin films on a large-area transparent substrate (Figure 2c). The crystallinity and its porosity of the nHKUST-1 film were completely preserved (Figure 2a,b). The existence of graphene as a physical mixture with nHKUST-1 in the film was evident by measuring the Raman spectrum in three regions (labeled A−C in Figure 2c). The spectrum showed peaks at 1350 and 1583−1616 cm^{-1} for defect (D band) and in-plane vibration (G band), corresponding to the sp^2 carbon atoms of graphene (Figure 2d).[26] The SEM image of nHKUST-1 film showed a flat 2 μm thick film, and transmission electron microscopy (TEM) showed particles of graphene distributed as a minority constituent in the nHKUST-1 film (Supporting Information, Figure S17).

For the fabrication of the nMOF supercapacitor, two nHKUST-1 films were sandwiched with a separator (monolayer polypropylene separator membranes, thickness 25 μm, Celgard) in a coin-shaped cell and soaked

TABLE 1. Summary of the Maximum Stack and Areal Capacitance and Life Cycle for All nMOFs and Related Supercapacitors

nMOF/material	max stack capacitance ($F\ cm_{stack}^{-3}$)	max areal capacitance ($mF\ cm_{areal}^{-2}$)	life cycle[d]
nMOF-5	0.043	0.341	3500
nMTV-MOF-5-AB	0.029	0.232	10000
nMTV-MOF-5-AC	0.060	0.478	1600
nMTV-MOF-5-AD	0.072	0.566	>10000
nMTV-MOF-5-AE	0.122	0.913	3000
nMTV-MOF-5-AF	0.025	0.195	>10000
nMTV-MOF-5-ABC	0.100	0.790	3500
nMTV-MOF-5-ABCD	0.113	0.891	>10000
nMTV-MOF-5-ABCDE	0.095	0.752	2500
nMTV-MOF-5-ABCDEF	0.063	0.501	1500
nNi-MOF-74	0.052	0.415	4000
nCo-MOF-74	0.050	0.392	>10000
nM3M-MOF-74	0.056	0.443	4000
nM5M-MOF-74	0.106	0.834	800
nM7M-MOF-74	0.146	1.155	300
nHKUST-1	0.296	2.334	6000
nHKUST-1-NG[a]	0.041	0.324	
Cu-BTC-NPNC[b]	0.028	0.221	
nMOF-177	0.090	0.713	4000
nZIF-8	0.034	0.268	2500
nMOF-801	0.280	2.329	1400
nMOF-801-L[c]	0.036	0.284	1500
nUiO-66	0.246	1.945	7000
nUiO-67	0.093	0.736	>10000
nMOF-867	**0.644**	**5.085**	**>10000**
nMOF-808	0.068	0.540	5000
activated carbon	**0.100**	**0.788**	**>10000**
graphene	0.065	0.515	>10000

[a] NG, no graphene. [b] NPNC, no porosity and no crystallinity. [c] L, large-size nanocrystals. [d] The life cycle was determined by the number of cycles carried out until the capacitance dropped to 80% of the initial value.

with a 1 M solution of tetraethylammonium tetrafluoroborate, $(C_2H_5)_4NBF_4$, in acetonitrile. The diameter of $(C_2H_5)_4N^+$ and BF_4^- is 0.68 and 0.33 nm, respectively.[27] After the coin-shaped cell was sealed, charge/discharge profiles, cyclic voltammetry (CV), and life cycle were all measured by galvanostatic measurements. Charge/discharge profiles of the nHKUST-1 supercapacitor were first measured to give its capacitance, energy, and power density in the various current densities with the potential swept in a range of the cutoff values ($0 \leq E \leq 2.7$ V). All values were calculated in volumetric and areal performance of the stack (this includes a pair of active material and substrate, and the separator)[28] (Supporting Information). Measurements of CV and cycling profile were followed to investigate its electrochemical behavior and life cycle. The capacitance is plotted as a function of current density in Figure 3, and values of the maximum stack and areal capacitance and life cycle for all nMOF supercapacitors are listed in Table 1. In addition, galvanostatic, CV curves, and cycle profiles for all nMOF supercapacitors are presented in the Supporting Information.

DISCUSSION

The pore environment produced by multiple functionalities clearly influences the capacitance in the nMTV-MOF-5 series (Figure 3a,b and Table 1). Combinations containing C, D, or E functionalities outperform others with A, B, or F. The F functionality leads to poor performance, most likely because it blocks the pores as shown in their N_2 adsorption data (Supporting Information, Figure S2), while C, D, and E combinations are relatively better. However, the capacitance of this entire series is lower than that observed for activated carbon. MOF-74 has a metal oxide backbone linked by organic units and is known to incorporate multiple metal ions without changing the MOF structure (Supporting Information, Figures S5 and S6 and Table S1). Mixing more than three metals in this MOF series (Figure 3c and Table 1) gives better performance than the original unmixed ones, which is attributed to redox reactions in charge/discharge process as observed in their CV profiles (Supporting Information, Figure S53−S57). In general, these highly mixed metal compounds perform better than any of the nMTV-MOF-5 members. This is in contrast to the inferior performance of the nanocrystals of MOF-177 and ZIF-8 (Figure 3d). An important MOF is HKUST-1 because it has three-dimensional pores with open metal sites in the backbone structure that point into the pores. The performance of nHKUST-1 is better than that of both the MTV-MOF-5 and MOF-74 series, and its maximum capacitance is three times that of activated carbon (Figure 3d and Table 1). We believe that the crystallinity and porosity of nMOFs contribute to their high performance: we synthesized a nonporous and noncrystalline Cu-BTC-NPNC, which has the same constituents as nHKUST-1, and found that it gave very low capacitance (Figure 3d and Table 1). The use of nHKUST-1 without doping with graphene (nHKUST-1-NG) also gives very low capacitance and points to the key role doped graphene plays in enhancing electron mobility within these devices. However, control experiments with increased ratios of graphene in the nHKUST-1 film show decreased capacitance (Supporting Information), which further confirms the importance of the nMOFs as the active material giving the high performance.

Members of a new class of chemically and thermally stable MOFs based on zirconium(IV) show progressively better performance as pore diameter decreased from nUiO-67 (9.6 and 12.6 Å) to nUiO-66 (6.8 and 7.2 Å) to nMOF-801 (5.4 and 7.0 Å) with the latter two exhibiting higher performance than any of the MOFs already discussed. Meanwhile, nMOF-808 having two different pore diameters (4.6 and 18.4 Å) is found to give an intermediate performance. It is worth noting that for films based on nMOF-801 with different nanocrystal sizes (nMOF-801 and nMOF-801-L with 100 and 500 nm, respectively), a lower performance is observed for the larger nanocrystals (Figure 3e and Table 1).

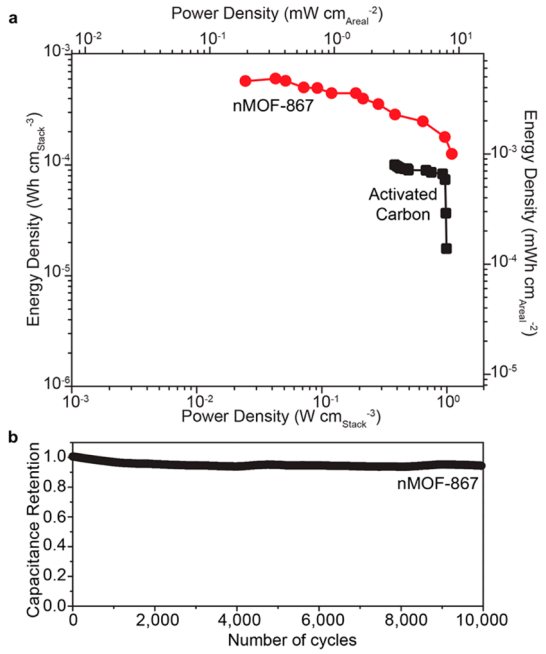

Figure 4. Energy and power densities and life cycle for supercapacitors: (a) Energy and power densities of nMOF-867 compared with activated carbon; (b) life cycle for nMOF-867.

Remarkably, we found that using nMOF-867 whose structure is the same as nUiO-67 but with 2,2′-bipyridine instead of biphenyl gives the highest performance (Figure 3f and Table 1). The capacitance of this material (0.644 F cm_{stack}^{-3} and 5.085 mF cm_{areal}^{-2}) is over 6 and 10 times that of activated carbon (0.100 F cm_{stack}^{-3} and 0.788 mF cm_{areal}^{-2}) and graphene (0.065 F cm_{stack}^{-3} and 0.515 mF cm_{areal}^{-2}), respectively. The gravimetric capacitance of nMOF-867 is 726 F $g_{nMOF\text{-}867/electrode}^{-1}$ (Supporting Information). The maximum energy and power densities of nMOF-867 are 6.04×10^{-4} Wh cm_{stack}^{-3} (3.85×10^{-3} mWh cm_{areal}^{-2}) and 1.097 W cm_{stack}^{-3} (8.67 mW cm_{areal}^{-2}), respectively (Figure 4a). At the power density of 0.386 W cm_{stack}^{-3}, the energy density (2.86×10^{-4} Wh cm_{stack}^{-3}) of nMOF-867 is over three times that of activated carbon (1.00×10^{-4} Wh cm_{stack}^{-3}). Moreover, at this power density, nMOF-867 consistently preserves its performance for at least 10000 cycles under the condition of extended exposure to the maximum voltage (0−2.7 V) (Figure 4b). Considering the similarity in chemical composition, crystal structure, porosity (Supporting Information), and electrochemical behavior observed in the CV data (Supporting Information, Figures S61 and S62) of nUiO-67 and nMOF-867, it is noteworthy that the sp^2 nitrogen atoms in nMOF-867 contribute to increase the interaction with ions significantly and enhanced the device performance.[29,30]

CONCLUSION

We targeted 23 porous metal−organic frameworks representing a diversity of structure types and metrics, and sizes and functionalities of pores, for their synthesis in nanocrystalline form and study of their performance and properties as supercapacitors. It is significant that the charge/discharge profiles (Supporting Information, Figures S19−S42), CV curves (Supporting Information, Figures S43−S66), and cycling performance (Supporting Information, Figures S67−S90) of these nMOFs follow the general behavior observed in other supercapacitors.[1−7] The differences are in the details of the nMOF electrochemical behavior; perhaps their diverse structural and functionality attributes are directly involved in electrochemical processes, and depending on their chemical nature, some undergo redox reactions, which makes several of these nMOFs exceed the capacitance of the benchmark materials. Future work will focus on deciphering the specific impact of these factors on the observed high capacitance of nMOFs.

METHODS

Preparation of nMOFs. Detailed synthetic procedures for all nMOFs are described in the Supporting Information. Here, we describe the preparation method for nHKUST-1, representatively. A 126 mg portion of 1,3,5-benzenetricarboxylic acid ($BTCH_3$) and 0.25 mL of triethylamine were dissolved in 2 mL of *N*,*N*-dimethylformamide (DMF), while 215 mg of $Cu(OAc)_2 \cdot H_2O$ was dissolved in 5 mL of DMF. The solutions of 1,3,5-benzenetricarboxylic acid and $Cu(OAc)_2 \cdot H_2O$ was combined in a mixture of DMF (18 mL), EtOH (25 mL), and H_2O (25 mL) and stirred vigorously for 1 h at ambient temperature. The resultant nHKUST-1 was washed twice with DMF using a centrifuge (9000 rpm for 20 min) and sonication and then sequentially immersed in acetone for three 24 h periods. Finally, nHKUST-1 was activated by removing the solvent under vacuum overnight.

Preparation of nMOF Films. A 70 mg portion of the nMOF was mixed and dispersed with 53 μL of oleic acid in 4.6 mL of hexane (nMOF/hexane dispersion) by sonication for 3 h. At the same time, graphene layers (0.5 mg mL^{-1}) were separated in hexane by using a tip-sonic processor for a total of 40 min (4 × 10 min operation) and continuously sonicated in the ultrasonic bath (40 kHz) to keep their dispersion (graphene/hexane dispersion). After the nMOF was separated from 1 mL of nMOF/hexane dispersion using a centrifuge (9000 rpm, 10 min), it was redispersed in 1 mL of graphene/hexane dispersion (0.5 mg mL^{-1}) to make a nMOF and graphene dispersion in hexane (nMOF/graphene/hexane dispersion). In the meantime, substrates were cleaned with hypophosphorous acid (50 wt % solution in water) for 1 h after washing with acetone, ethanol, and water. The nMOF/graphene/hexane dispersion was coated on the cleaned substrates in the spin coater (7000 rpm, 2 min) to give a 2 μm thickness of nMOF film. Oleic acid was removed by immersing the nMOF film in acetone, drying with nitrogen flow, and outgassing at room temperature for 12 h. All processes were done in succession.

Fabrication of Supercapacitors. For the fabrication of supercapacitors, two nMOF film samples, separator and electrolyte, were assembled in a coin-shaped cell. Specifically, two pieces of nMOF film (2 μm) on Ti substrates (25 μm) were sandwiched with a separator (monolayer polypropylene separator membranes, thickness 25 μm, Celgard) and soaked in 1.0 M of tetraethylammonium tetrafluoroborate ($(C_2H_5)_4NBF_4$) in acetonitrile. After

the coin-shaped cell was sealed, supercapacitors were electrochemically tested using galvanostatic and cyclic voltammetry measurements. The same method was applied for all of the supercapacitors in this paper.

Conflict of Interest: The authors declare no competing financial interest.

Acknowledgment. This research was supported by BASF SE (Ludwigshafen, Germany) at UC Berkeley, the Global Frontier R&D Program (2013-073298) of the Center for Hybrid Interface Materials (HIM), and the National Research Foundation of Korea (2011-0028737) at KAIST-Korea. We thank J. Jiang, H. Bae, L. Wang, and H. Furukawa for help in the nMOF synthesis and invaluable discussions.

Supporting Information Available: Detailed preparation procedure and characterization by X-ray diffraction analysis, low-pressure nitrogen sorption, ^{1}H NMR spectroscopy, ICP–OES (inductively coupled plasma-optical emission spectroscopy), SEM and TEM imaging for nMOFs and nMOF films, fabrication and data collection procedure and electrochemical data (charge/discharge profiles, cyclic voltammetry data, life cycle and control experiments data with different amount of graphene) for nMOF supercapacitors. This material is available free of charge *via* the Internet at http://pubs.acs.org.

REFERENCES AND NOTES

1. Conway, B. E. *Electrochemical Supercapacitors: Scientific Fundamentals and Technological Applications*; Kluwer-Academic/Plenum-Publisher: New York, 1999.
2. Simon, P.; Gogotsi, Y. Materials for Electrochemical Capacitors. *Nat. Mater.* **2008**, *7*, 845–854.
3. El-Kady, M. F.; Strong, V.; Dubin, S.; Kaner, R. B. Laser Scribing of High-Performance and Flexible Graphene-Based Electrochemical Capacitors. *Science* **2012**, *335*, 1326–1330.
4. Chmiola, J.; Largeot, C.; Taberna, P. L.; Simon, P.; Gogotsi, Y. Monolithic Carbide-Derived Carbon Films for Micro-Supercapacitors. *Science* **2010**, *328*, 480–483.
5. Zhu, Y.; Murali, S.; Stoller, M. D.; Ganesh, K. J.; Cai, W.; Ferreira, P. J.; Pirkle, A.; Wallace, R. M.; Cychosz, K. A.; Thommes, M.; et al. Carbon-Based Supercapacitors Produced by Activation of Graphene. *Science* **2012**, *332*, 1537–1541.
6. Brezesinski, T.; Wang, J.; Tolbert, S. H.; Dunn, B. Ordered Mesoporous Alpha-MoO_3 with Iso-Oriented Nanocrystalline Walls for Thin-Film Pseudocapacitors. *Nat. Mater.* **2010**, *9*, 146–151.
7. Yu, G.; Hu, L.; Liu, N.; Wang, H.; Vosgueritchian, M.; Yang, Y.; Cui, Y.; Bao, Z. Enhancing the Supercapacitor Performance of Graphene/MnO_2 Nanostructured Electrodes by Conductive Wrapping. *Nano Lett.* **2011**, *11*, 4438–4442.
8. Wang, H.; Casalongue, H. S.; Liang, Y.; Dai, H. $Ni(OH)_2$ Nanoplates Grown on Graphene as Advanced Electrochemical Pseudocapacitor Materials. *J. Am. Chem. Soc.* **2010**, *132*, 7472–7477.
9. Furukawa, H.; Cordova, K. E.; O'Keeffe, M.; Yaghi, O. M. The Chemistry and Applications of Metal-Organic Frameworks. *Science* **2013**, *341*, 974.
10. Snook, G. A.; Kao, P.; Best, A. S. Conducting-Polymer-Based Supercapacitor Devices and Electrodes. *J. Power Sources* **2011**, *196*, 1–12.
11. Diaz, R.; Orcajo, M. G.; Botas, J. A.; Calleja, G.; Palma Co8-MOF-5 as Electrode for Supercapacitors. *J. Mater. Lett.* **2012**, *68*, 126–128.
12. Allendorf, M. D.; Schwartzberg, A.; Stavila, V.; Talin, A. A. A Roadmap to Implementing Metal–Organic Frameworks in Electronic Devices: Challenges and Critical Directions. *Chem.—Eur. J.* **2011**, *17*, 11372–11388.
13. Li, H.; Eddaoudi, M.; O'Keeffe, M.; Yaghi, O. M. Design and Synthesis of an Exceptionally Stable and Highly Porous Metal-Organic Framework. *Nature* **1999**, *402*, 276–279.
14. Deng, H.; Doonan, C. J.; Furukawa, H.; Ferreira, R. B.; Towne, J.; Knobler, C. B.; Wang, B.; Yaghi, O. M. Multiple Functional Groups of Varying Ratios in Metal–Organic Frameworks. *Science* **2010**, *327*, 846–850.
15. Glover, T. G.; Peterson, G. W.; Schindler, B. J.; Britt, D.; Yaghi, O. MOF-74 Building Unit Has a Direct Impact on Toxic Gas Adsorption. *Chem. Eng. Sci.* **2011**, *66*, 163–170.
16. Wang, L. J.; Deng, H.; Furukawa, H.; Gándara, F.; Cordova, K. E.; Peri, D.; Yaghi, O. M. Synthesis and Characterization of Metal–Organic Framework-74 Containing 2, 4, 6, 8, and 10 Different Metals. *Inorg. Chem.* **2014**, *53*, 5881–5883.
17. Wißmann, G.; Schaate, A.; Lilienthal, S.; Bremer, I.; Schneider, A. M.; Behrens, P. Modulated Synthesis of Zr-fumarate MOF. *Microporous Mesoporous Mater.* **2012**, *152*, 64–70.
18. Cavka, J. H.; Jakobsen, S.; Olsbye, U.; Guillou, N.; Lamberti, C.; Bordiga, S.; Lillerud, K. P. A New Zirconium Inorganic Building Brick Forming Metal Organic Frameworks with Exceptional Stability. *J. Am. Chem. Soc.* **2008**, *130*, 13850–13851.
19. Li, L.; Tang, S.; Wang, C.; Lv, X.; Jiang, M.; Wu, H.; Zhao, X. High Gas Storage Capacities and Stepwise Adsorption in a UiO Type Metal–Organic Framework Incorporating Lewis Basic Bipyridyl Sites. *Chem. Commun.* **2014**, *50*, 2304–2307.
20. Furukawa, H.; Gándara, F.; Zhang, Y.-B.; Jiang, J.; Queen, W. L.; Hudson, M. R.; Yaghi, O. M. Water Adsorption in Porous Metal-Organic Frameworks and Related Materials. *J. Am. Chem. Soc.* **2014**, *136*, 4369–4381.
21. Chui, S. S.-Y.; Lo, S. M.-F.; Charmant, J. P. H.; Orpen, A. G.; Williams, I. D. A Chemically Functionalizable Nanoporous Material $[Cu_3(TMA)_2(H_2O)_3]_n$. *Science* **1999**, *283*, 1148–1150.
22. Chae, H. K.; Siberio-Pérez, D. Y.; Kim, J.; Go, Y.; Eddaoudi, M.; Matzger, A. J.; O'Keeffe, M.; Yaghi, O. M. A Route to High Surface Area, Porosity and Inclusion of Large Molecules in Crystals. *Nature* **2004**, *427*, 523–527.
23. Park, K. S.; Ni, Z.; Côté, A. P.; Choi, J. Y.; Huang, R.; Uribe-Romo, F. J.; Chae, H. K.; O'Keeffe, M.; Yaghi, O. M. Exceptional Chemical and Thermal Stability of Zeolitic Imidazolate Frameworks. *Proc. Natl. Acad. Sci. U.S.A.* **2006**, *103*, 10186–10191.
24. Britt, D.; Furukawa, H.; Wang, B.; Glover, T. G.; Yaghi, O. M. Highly Efficient Separation of Carbon Dioxide by a Metal-Organic Framework Replete with Open Metal Sites. *Proc. Natl. Acad. Sci. U.S.A.* **2009**, *106*, 20637–20640.
25. Rowsell, J. L. C.; Yaghi, O. M. Effects of Functionalization, Catenation, and Variation of the Metal Oxide and Organic Linking Units on the Low-Pressure Hydrogen Adsorption Properties of Metal–Organic Frameworks. *J. Am. Chem. Soc.* **2006**, *128*, 1304–1315.
26. Kudin, K. N.; Ozbas, B.; Schniepp, H. C.; Prud'homme, R. K.; Aksay, I. A.; Car, R. Raman Spectra of Graphite Oxide and Functionalized Graphene Sheets. *Nano Lett.* **2008**, *8*, 36–41.
27. Chmiola, J.; Yushin, G.; Gogotsi, Y.; Portet, C.; Simon, P.; Taberna, P. L. Anomalous Increase in Carbon Capacitance at Pore Sizes Less Than 1 Nanometer. *Science* **2006**, *313*, 1760–1763.
28. Gogotsi, Y.; Simon, P. True Performance Metrics in Electrochemical Energy Storage. *Science* **2011**, *334*, 917–918.
29. Wang, H.; Maiyalagan, T.; Wang, X. Review on Recent Progress in Nitrogen-Doped Graphene: Synthesis, Characterization, and Its Potential Applications. *ACS Catal.* **2012**, *2*, 781–794.
30. Jeong, H. M.; Lee, J. W.; Shin, W. H.; Choi, Y. J.; Shin, H. J.; Kang, J. K.; Choi, J. W. Nitrogen-Doped Graphene for High-Performance Ultracapacitors and the Importance of Nitrogen-Doped Sites at Basal Planes. *Nano Lett.* **2011**, *11*, 2472–2477.